Proceedings of the ASME 2014 Conference on Smart Materials, Adaptive Structures and Intelligent Systems SMASIS2014

September 8-10, 2014, Newport, Rhode Island, USA

# **SMASIS2014-7528**

# STABILITY ANALYSIS OF THE WING LEADING EDGE SPAR OF A PASSIVELY MORPHING ORNITHOPTER

# **Aimy Wissa**

Department of Aerospace Engineering University of Maryland College Park, MD, USA

James E. Hubbard Jr.

Department of Aerospace Engineering University of Maryland College Park, MD, USA

#### **ABSTRACT**

This paper presents a stability model for the wing leading edge spar of a test ornithopter. The long-term goal of this research effort is to passively improve the performance of ornithopters during steady level flight by implementing a set of wing kinematics found in natural flyers. The desired kinematics is achieved by inserting a compliant mechanism called a compliant spine into the wing leading edge spar to mimic the function of an avian wrist. The stiffness of the compliant spine is time varying and given the nature of flapping flight, it is periodic. Introducing a variable stiffness compliant mechanism into the leading edge spar of the ornithopter affects its structural stability. Therefore, a stability analysis is required. In order to start the stability analysis, an analytical model of the ornithopter wing leading edge spar with a compliant spine inserted in is necessary. In the model, the compliant spine is modeled as a torsional spring with a sinusoidal stiffness function. Moreover, the equations of motion of the wing leading edge spar-spine system can be written in the form of nonhomogeneous Mathieu's equations, which has well-known stability criteria. The analytical system response is then validated using experimental data taken at NASA Langley Research Center. Results show that the analytical spine angular deflection agrees with the experimental angular deflection data within 11%. Stability was then

# Joseph Calogero

Dept. of Mechanical and Nuclear Engineering The Pennsylvania State University University Park, PA, USA

# **Mary Frecker**

Dept. of Mechanical and Nuclear Engineering The Pennsylvania State University University Park, PA, USA

demonstrated using both analytical and graphical proving that the response of leading edge spar with a compliant spine design inserted at 37% of the wing half span is bounded.

#### I. INTRODUCTION

During the last few decades, flapping wing Unmanned Aerial Vehicles (UAVs), or ornithopters, have shown the potential for advancing and revolutionizing UAV performance in both the civil and military sectors[1]. An ornithopter is unique in that it can combine the agility and maneuverability of rotary wing aircraft with excellent performance in low Reynolds number flight regimes. These traits could yield optimized performance over multiple mission scenarios. Nature achieves such performance in birds using wing gaits that are optimized for a particular flight condition [2],[3]. The desired bioinspired kinematics that we want to implement on a test ornithopter to improve steady level flight is known as the Continuous Vortex Gait (CVG). A detailed discussion of the kinematics of the CVG can be found in [2] and [3]. The advantage of using the CVG is that it is an avian gait that can be implemented passively and requires motion in only one major joint, namely the wrist. The desired bending kinematics of the CVG can be achieved by inserting a contact-aided compliant mechanism called a compliant

spine into the wing leading edge spar to mimic the function of an avian wrist. The compliant spine is inserted in the leading edge spar of the test ornithopter wings at 37% of the wing half span, as shown in Figure 1. The compliant spine is designed to be flexible during the upstroke, while remaining stiff during the downstroke, as shown in Figure 2. References 4, 5, and 6 detail the design optimization of the compliant spine. The stiffness of the compliant spine is time varying and, given the nature of steady-level flapping flight, it is also periodic. Introducing a variable stiffness compliant mechanism into the leading edge spar of the ornithopter affects its structural stability. A stability analysis is thus required [7, 8].

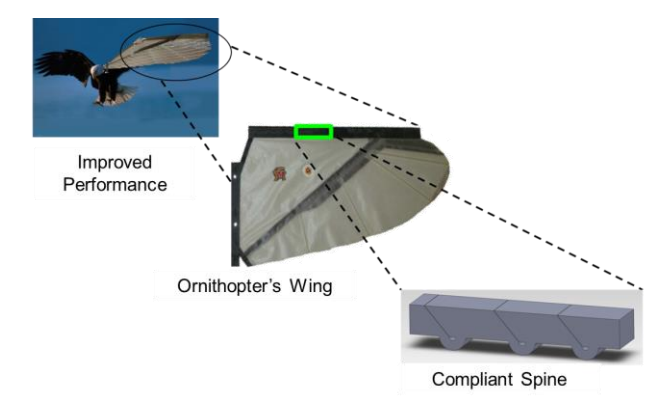


Figure 1. The compliant spine is inserted into the leading edge spar to mimic the function of an avian



Figure 2. The desired stiffness of the compliant spine is nonlinear. It is stiff in the downstroke, similar to a rigid spar, and flexible in the upstroke, similar to a torsional spring.

This paper presents a structural stability model for the wing leading edge spar of a test ornithopter. Modeling the wing leading edge spar with a compliant spine inserted in it yields linear time periodic equations of motion in the form of non-homogeneous Mathieu's equations. The model uses Floquet's decomposition [8, 9] to determine the stability of the leading edge (LE) spar using graphical and analytical methods with various compliant spine designs inserted in it. The remainder of the paper is organized as follows:

Section 2 presents the equations of motion for the leading edge spar, Section 3 explains the experimental validation for the model, Section 4 discusses the stability analysis, and Section 5 includes conclusions and future work.

# 2. LEADING EDGE SPAR EQUATIONS OF MOTION

# 2.1 Research Platform Specifications

The leading edge spar modeled in this paper is the main spar of an avian scale flapping wing un-manned air vehicle. Figure 3 shows a picture of the research platform and Table 1 includes the specifications [10]. The ornithopter wings consist of the leading edge spar, a wing membrane, a diagonal spar and five finger spars as shown in Figure 4. The leading edge spar is the spar connected to the wing root and the flapping mechanism. It is a unidirectional carbon fiber rod with a 3.96 m diameter.



Figure 3. Test Platform

Table 1. Ornithopter specification that are common across all configurations

Specification	Value
Span	1.07 m
Flapping Rate	4 – 6 Hz
Speed	2.5 - 8.5 m/s
Max. Chord	0.28 m
Range	0.8 km
Wing Stroke Angle	1.17 rad



Figure 4: Top view of the research platform wings with its components labeled.

The compliant spine is designed to mimic the function of an avian wrist, thus it is inserted in the leading edge. The compliant spine is attached to the carbon fiber spar using six 5-40 bolts and a Delrin collar, as shown in Figure 5.

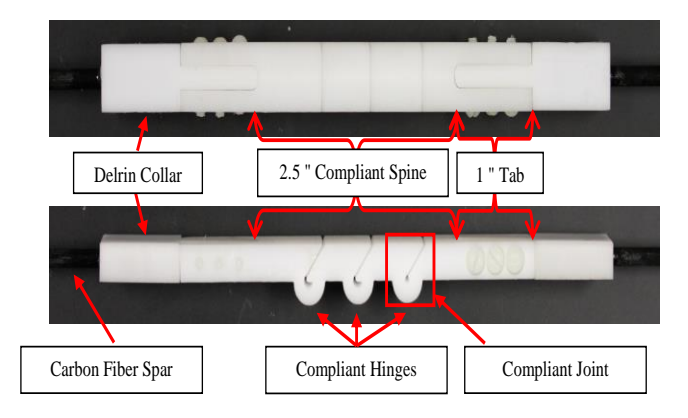


Figure 5. Compliant spine assembly components

#### 2.2 Leading Edge Spar Model

The leading edge spar is modeled as two rigid rods. One rod is inboard to the compliant spine and the other is outboard to the compliant spine. The boundary conditions for these rods are shown in Figure 6. The inboard rod has a pinned boundary condition at the root and is connected to the torsional spring on the other end. The outboard rod has a free boundary condition at the wing tip and is connected to the torsional spring on one end. The compliant spine is modeled as a torsional spring with a sinusoidal stiffness function. The torsional stiffness of the spring representing the compliant spine is described as:

$$k_{T} = (k_{a} + k_{b}) - k_{b} cos(\frac{2\pi t}{T})$$
 (1)

where,

$$k_a = k_u \tag{2}$$

$$k_b = \frac{k_d - k_u}{2} \tag{3}$$

In the equations above,  $k_u$  and  $k_d$  are the upstroke and downstroke stiffness of the compliant spine in Newton-meter per radian, respectively, t is time in seconds, and T is the period of one wing beat cycle. The values of  $k_u$  and  $k_d$  are determined based on the compliant spine design choice.

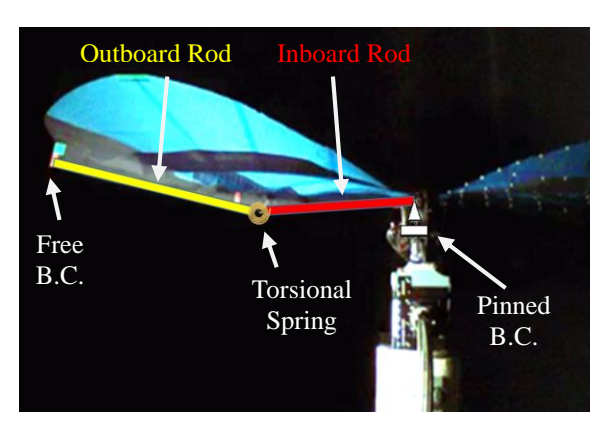


Figure 6. The research platform mounted on a test stand with the leading edge spar model superimposed on the right wing for clarification.

Figure 7 shows a schematic of the leading edge spar-spine system. In this figure,  $\theta_1$  is the wing root angle,  $\theta_2$  is the spine root angle,  $L_1$  and  $m_1$  are the length and mass of the inboard rod,  $L_2$  and  $m_2$  are the length and mass of the outboard rod, and M is motor torque.

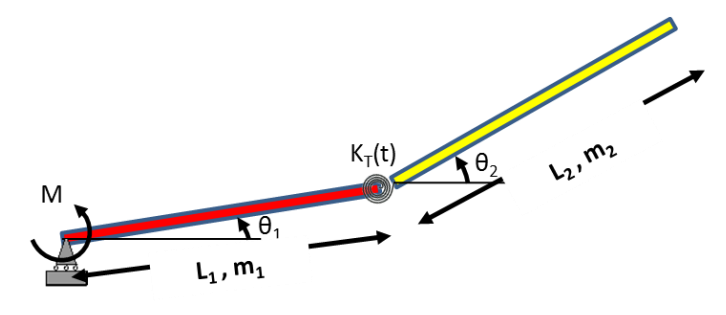


Figure 7. Detailed model of the leading edge spar showing all relevant angles, lengths, and masses.

In the above diagram,  $\theta_1$  is the prescribed wing root angle. Equation 4 shows the expression for  $\theta_1$ .

$$\theta_1 = \frac{\varphi}{2} \sin(\omega t) \tag{4}$$

where,  $\varphi$  is the wing stroke angle, and  $\omega$  is the flapping frequency in radians per second.

Using Newton's principles, one can derive the equations of motion (EOM) of the two rods shown in Figure 7. Equations 5 and 6 list the EOM of the system.

$$\begin{split} I_{A}\ddot{\theta_{1}} - k_{T}[\theta_{2} - \theta_{1}] + m_{2}\ddot{y}_{2 \text{ c.m.}} L_{1}\cos\theta_{1} \\ - m_{2}\ddot{x}_{2 \text{ c.m.}} L_{1}\sin\theta_{1} = M \end{split} \tag{5}$$

$$I_B \ddot{\theta_2} + k_T [\theta_2 - \theta_1] = 0$$
 (6)

where,  $I_A$  and  $I_B$  are the mass moment of inertia of the inboard and outboard rods, respectively and  $\ddot{x}_{2\ c.m.}$  and  $\ddot{y}_{2\ c.m.}$  are the horizontal and vertical accelerations of the center of mass of the outboard rod, respectively.

Equations 5 and 6 are decoupled since the wing root angle is prescribed. Therefore, one can solve Equation 6 directly for the spine root angle  $(\theta_2)$ . Equation 5 then becomes a compatibility equation describing the amount of torque the motor has to produce in order to drive the system at the prescribed wing root angle  $(\theta_1)$ . Matlab's® general forward time integration function, ODE45, was used to solve Equation 6 numerically. Section 3 compares the analytically calculated wing root and spine root angles with their experimentally measured counterparts.

# 3. LEADING EDGE SPAR MODEL VALIDATION

# 3.1 Experimental Set-up

Experimental data is used to validate the aforementioned model of the leading edge spar. Details about the experiment can be found in [11]. The test took place at NASA Langley Research Center (LaRC) thermal vacuum laboratory inside a 5 foot x 5 foot thermal vacuum chamber. The thermal vacuum chamber is capable of providing a pressure range from atmospheric pressure of 760 Torr to altitude vacuum and thermal simulation of approximately 10 E-7 Torr. Figures 8a and 8b show the 5' x 5' foot thermal vacuum chamber and the test ornithopter mounted inside the vacuum chamber, respectively.



(a)



(b)

Figure 8. a) NASA LaRC 5 foot x 5 foot thermal vacuum chamber. b) Test ornithopter mounted inside the vacuum chamber.

In order to capture the deflection, four retro-reflective markers are placed at the leading edge. One marker is placed at the wing root, a second one is placed at the location of the compliant spine root, a third marker is placed at the location of the compliant spine tip, and a fourth marker is placed at the wing tip. The kinematics are captured using a Phantom V9.1 high speed camera at 200 frames per second. The camera is mounted outside of the vacuum chamber as shown in Figures 8a and 9a. In order to illuminate the markers for tracking purposes, 3 LED light panels are mounted on the inside of the vacuum chamber as shown in Figure 9b. Figure 9c shows a picture of how the leading edge markers appear when the chamber door is closed and the LED panels are lit.

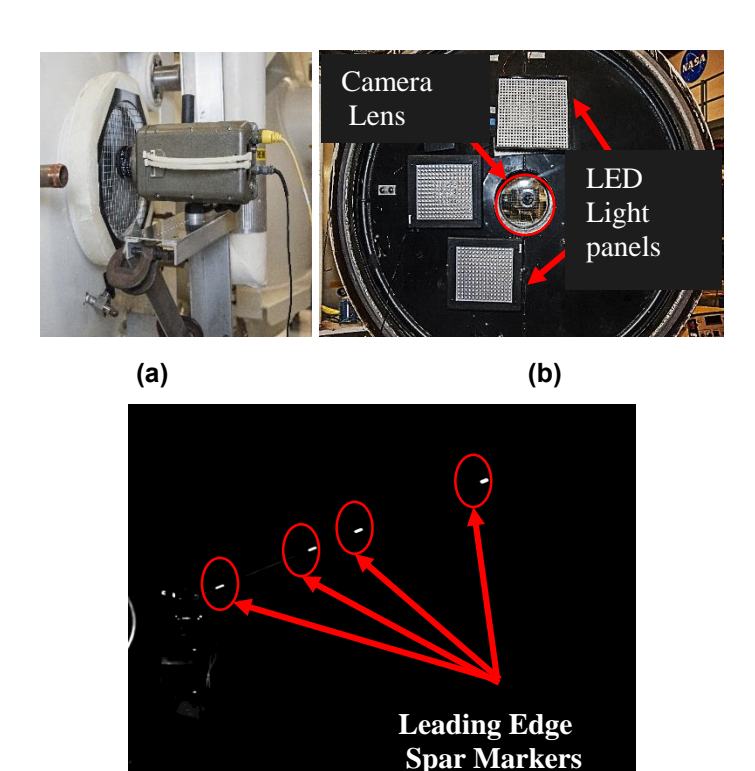


Figure 9. a) A Phantom high speed camera mounted outside the vacuum chamber. b) 3 LED panels mounted on the inside of the chamber to light the chamber and cause the markers to reflect light. c) A sample video frame of the leading edge retro reflective markers when the chamber is closed and the LED light panels are lit.

(c)

## 3.2 Experimental Validation of Leading Edge Spar

The experiment described in Section 3.1 is conducted using the same assumptions and constraints used to develop the model. Thus, the experimental data used is taken in vacuum at a pressure of 1Torr because the model does not include aerodynamic effects. The wing-spar configuration used to validate the model consisted of the leading edge carbon fiber spar with compliant spine design Comp 4TL inserted at 37% of the wing half span. Figure 10a shows an example of a wing-spine configuration. Comp 4TL has an upstroke stiffness ( $k_u$ ) of 3.75 N-m/rad and a downstroke stiffness ( $k_d$ ) of 72.5 N-m/rad. Figure 10b shows a schematic of compliant spine design, Comp 4TL. During the experiment, the leading edge of the ornithopter was flapped at 4.2 Hz. This flapping frequency is suitable steady level flight.



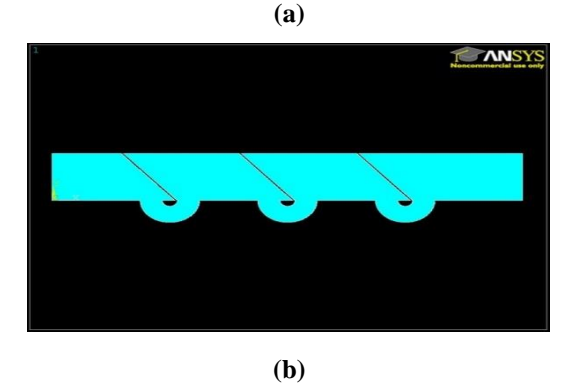


Figure 10. (a) Example of a leading edge spar-spine configuration. (b) A schematic of compliant spine design Comp 4TL.

The vertical displacement of the retro reflective markers is used to calculate the wing root  $(\theta_{1exp})$  and spine root  $(\theta_{2exp})$  angles, as shown by Equations 7 and 8.

$$\theta_{1exp} = \sin^{-1} \frac{[Y_{SR} - Y_{WR}]}{L_1} \tag{7}$$

$$\theta_{2exp} = \sin^{-1} \frac{[Y_{ST} - Y_{SR}]}{L_{spine}} \tag{8}$$

where,  $Y_{WR}$ ,  $Y_{SR}$ , and  $Y_{ST}$  are the vertical displacements of the wing root, spine root, and spine tip retro reflective markers respectively.  $L_{spine}$  is the compliant spine length which is 6.35 cm (2.5"). Figures 11 and 12 compare the experimental data with the model results. The error between the experimental data and the model is calculated using Equations 9 and 10.

$$RMSE_{\theta_1} = \sqrt{\frac{\sum_{1}^{n} \left(\theta_{1 exp} - \theta_1\right)^2}{n}} \approx 7 \% \tag{9}$$

$$RMSE_{\theta_2} = \sqrt{\frac{\sum_{1}^{n} (\theta_{2 \exp} - \theta_2)^2}{n}} \approx 11 \%$$
 (10)

where, n is the number of data points used over one flapping cycle.

The analytical wing root angle agrees within 7 % of the experimental data while the analytical spine root angle agrees within 11 % of the experimental data. The error observed in Figure 11 and Equation 9 is due to the assumption that the analytical wing root angle is sinusoidal. Experiment show that the wing root angle is not exactly sinusoidal. The wings spends more than half of the stroke below the horizontal plane. The error observed in Figure 12 and Equation 10 is attributed to the fact that any physical system has some structural damping, which is not accounted for in the model. Moreover, the model assumes that the carbon fiber spar is rigid while the physical carbon fiber spar has some flexibility. Finally the high frequency content noticed in the analytical spine root angle is typical of a bounded response of Mathieu's equation in which the ratio between the system's Eigen frequencies and frequency of excitation (flapping frequency) is small [12].

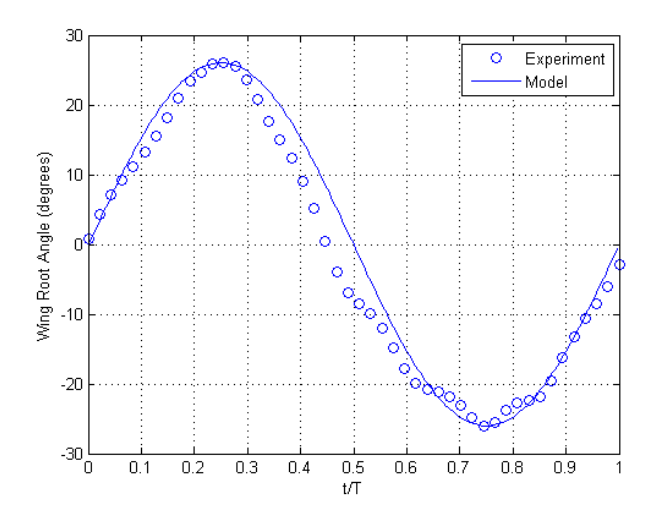


Figure 11. Experimental and analytical wing root angle versus time normalized by the period of one wing beat cycle. The experiment agrees with the model within 7%.

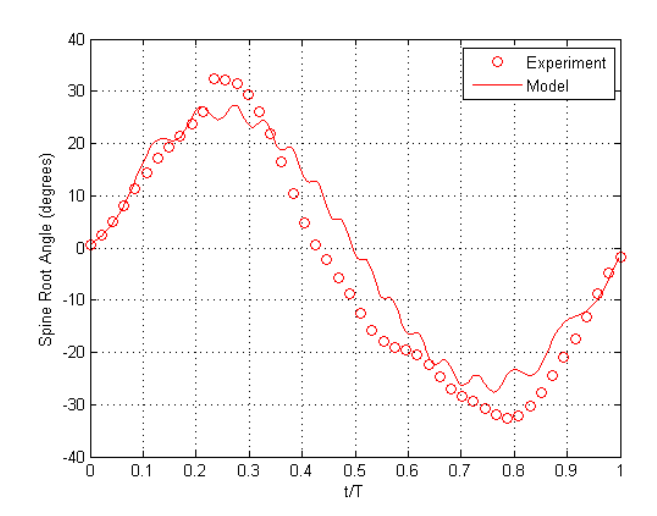


Figure 12. Experimental and analytical spine root angle versus time normalized by the period of one wing beat cycle. The experiment agrees with the model within 11%.

#### 4. STABILITY ANALYSIS

After validating the analytical model using experimental data as discussed in Section 3, the next step is to determine the structural stability of the leading edge spar with a compliant spine inserted in 37% of the wing half span. Equation 6 can be written in the form of a non-homogeneous Mathieu's equation, as shown by Equation 11. Equation 12 through 17 defines the symbols in Equation 11.

$$\ddot{\theta}_2(p) + [\delta + 2\epsilon \cos(2p)] \theta_2(p)$$

$$= [\alpha + 2\beta \cos(2p)] \sin(2p)$$
(11)

$$\delta = \frac{k_a + k_b}{A} \tag{12}$$

$$\epsilon = \frac{-k_b}{2A} \tag{13}$$

$$\alpha = \frac{\phi(k_a + k_b)}{2A} \tag{14}$$

$$\beta = \frac{-\phi k_b}{4A} \tag{15}$$

$$p = \frac{\pi t}{T} \tag{16}$$

$$A = \frac{I_B \pi^2}{T^2} \tag{17}$$

Mathieu's equation is a special form of Hill's equation. It is used to model parametrically excited system in which a parameter is varying periodically in a sinusoidal manner [9, 12, 13]. Several books and articles discuss the significance, history, and stability of Mathieu's equation [13]. The stability of a system written in the form of Mathieu's equation can be identified both graphically and analytically. The most common way to determine the stability of Mathieu's equation graphically is using the Strutt Diagram of the homogenous equation (see Equation 18). The non-homogeneous term on the right hand side of Equation 11 does not affect stability. A Strutt diagram is a plot of  $\delta$  versus  $\epsilon$  and the lines shown on the plot form boundaries between values of the parameters for which the solution is stable or unstable. Figure 12 shows the classical Strutt diagram of Mathieu's equation.

$$\ddot{\theta}_2(p) + [\delta + 2\epsilon \cos(2p)] \theta_2(p) = 0 \tag{18}$$

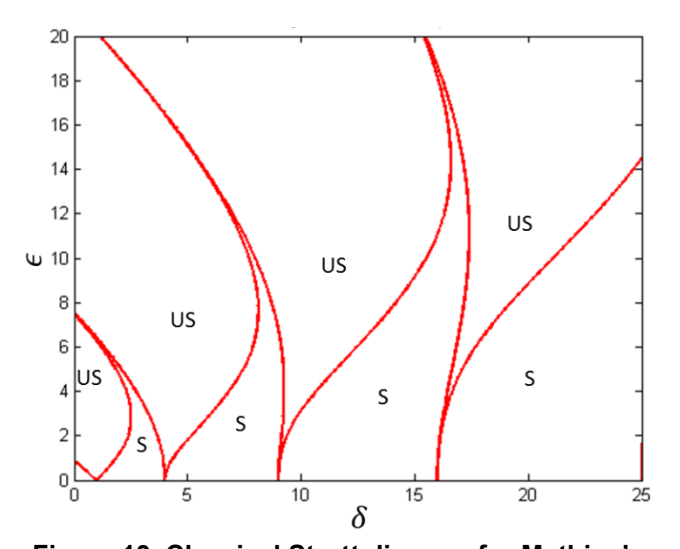


Figure 13. Classical Strutt diagram for Mathieu's equation. The lines form boundaries or transition point between stable and unstable solution regions. Regions marked with US are unstable and regions marked with S are stable.

The Strutt diagram in Figure 13 is in terms of  $\delta$  and  $\epsilon$ . Since the design parameters for the compliant spine are the upstroke and downstroke stiffness, it is useful to transform and plot the Strutt diagram above in terms of  $k_u$  and  $k_d$ . Figure 14 shows the transformed Strutt diagram. The figure also shows that design Comp 4TL which has an upstroke of 3.75 Nm/rad and downstroke stiffness of 72.5 Nm/rad, marked in the plot with a black dot, falls within a

stable region of the Strutt diagram. The figure demonstrates that the leading edge spar with design Comp 4TL is structurally stable.

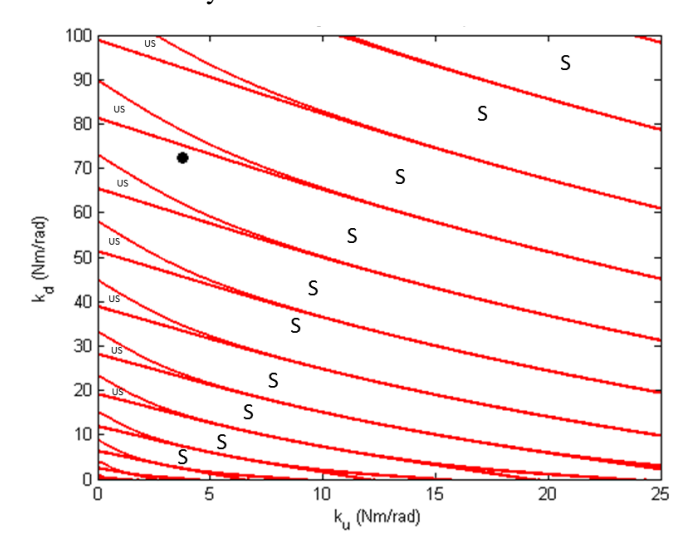


Figure 14. Classical Strutt diagram for Mathieu's equation. The black dot represents compliant spine Comp 4TL. Regions marked with US are unstable and regions marked with S are stable.

Figure 14 demonstrates stability graphically. Stability of Equation 11 can be also shown analytically by solving for the system response and examining the phase plane plot. The phase plane is a plot of the system response  $(\theta_2)$  versus its first derivative  $(\dot{\theta}_2)$ . Figure 15 shows the phase plane plot of Equation 11. The red dot in Figure 15 signifies the initial conditions given to the system. The plot shows that the response of leading edge spar with design Comp 4TL inserted at 37% of the wing half span is bounded and stable.

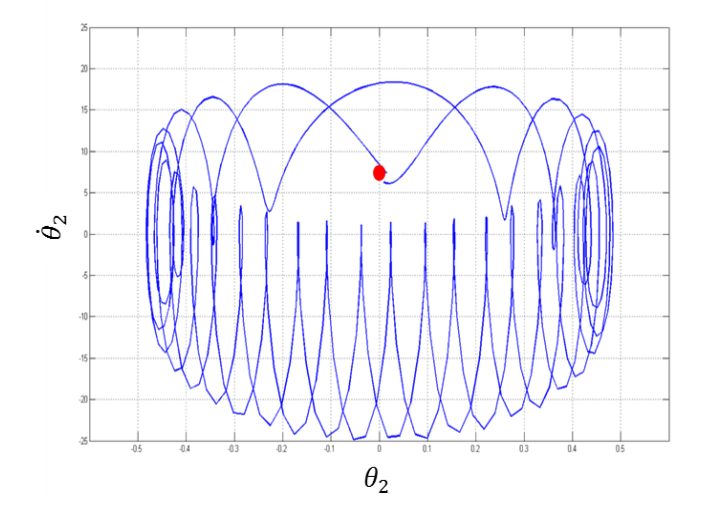


Figure 15. Phase plane plot of the spine root angle. The plot shows that the response of the leading edge spar with design Comp 4TL inserted at 37% of the wing half span is bounded and stable.

## **CONCLUSIONS**

The work presented in this paper demonstrated that the leading edge spar remained stable and its response remained bounded after inserting compliant spine design Comp 4TL at 37 % of the wing half span. In order to determine the stability of the spar-spine system, one of the systems equations of motion is written in Mathieu's equation form and the stability of the system is determined both graphically and analytically. The equations of motion and system response for a leading edge spar with a compliant spine mechanism that is designed to mimic the function of an avian wrist was derived and validated. The model was validated using bench-top experiments in vacuum performed at NASA Langley Research Center. Inserting the compliant spine into the leading edge spar has previously proved to be beneficial for steady level flight performance [14-16]. Future work includes confirming the structural stability of the leading edge spar with other compliant spine designs.

#### **ACKNOWLEDGMENTS**

The authors gratefully acknowledge the support of AFOSR grant number FA9550-09-1-0632 and FA9550-13-0126 under the direction of Dr. David Stargel. The computational work involving compliant spines was supported in part through instrumentation funded by the National Science Foundation through grant OCI–0821527. The resources of NASA Langley Research Center, the

University of Maryland, the Pennsylvania State University, and the Morpheus Lab are also appreciated.

## **REFERENCES**

- [1] Shyy, W. Berg, M., and Ljungqvist, D."Flapping and flexible wings for biological and micro air vehicles", Progress in Aerospace Sciences, (1999) 35: 455-505
- [2] Tobalske, B.W., and Dial, K.P. "Flight kinematics of Black-billed Magpies and pigeons over a wide range of speeds", Journal of Experimental Biology, (1996) 99: 263-280.
- [3] Tobalske, B.W. "Physiology and Biomechanics of Gait Selection in Flying Birds", Physiol Biochem Zool., (2000) 73(6):736-50.
- [4] Tummala, Y., Wissa A., Frecker, M., and Hubbard Jr., J. E. "Design of a passively morphing ornithopter wing using a novel compliant spine" Proc. Smart Materials, Adaptive Structures and Intelligent Systems Conf. 2010-3637, Philadelphia PA
- [5] Tummala, Y., Wissa, A., Frecker, M., and Hubbard Jr., J. E. "Design optimization of a compliant spine for dynamic applications," Proc. Smart Materials, Adaptive Structures and Intelligent Systems Conf. 2011-5207, Scottsdale, AZ
- [6] Tummala, Y., Wissa, A., Frecker, M., and Hubbard Jr., J. E " Design and optimization of a contact aided compliant mechanism for passive bending" Journal of Mechanics and Robotics (accepted manuscript)
- [7] Butikov, Eugene I. "Parametric excitation of a linear oscillator." *European Journal of Physics* 25 (2004): 535-554.
- [8] Simakhina, Svetlana. *Stability Analysis of Hill's Equation*. Thesis. U of Illinois at Chicago, 2003.
- [9] Wereley, Norman. Analysis and Control of Linear Periodically Time Varying Systems. Diss. Massachusetts Institute of Technology, 1991.
- [10] Harmon, Robyn. Aerodynamic Modeling of Flapping Membrane Wing Using Motion Tracking Experiments, Aerospace Engineering. Thesis. University of Maryland, 2009
- [11] Wissa, A., Tummala Y., Hubbard Jr., J. E., Frecker M, and Northrup M. "Inertial effects due to passive wing morphing in ornithopters" Proceedings of 22nd AIAA/ASME/AHS Adaptive Structures Conference, 2014, National Harbor, MD.
- [12] Nayfeh, Ali Hasan, and Dean T. Mook. *Nonlinear Oscillations*. New York: Wiley, 1979. Print.

- [13] McLachlan, N. W. Theory and Application of Mathieu Functions. Oxford: Clarendon, 1947. Print.
- [14] Wissa, A., Tummala, Y., Hubbard Jr., J. E., and Frecker, M. "Passively Morphing Ornithopter Wings using a Novel Compliant Spine: Design and Testing," Smart Materials and Structures (2102) 21094028
- [15] Wissa, A., Tummala Y., Hubbard Jr., J. E., Frecker M., and Brown, A. "Testing of novel compliant spines for passive wing morphing,"Proc. Smart Materials, Adaptive Structures and Intelligent Systems Conf. 2011-5198, Scottsdale, AZ
- [16] Wissa. A, Grauer J., Guerreiro, N., Tummala, Y., Roberts, R., Altenbuchner, C., Hubbard Jr., J., Frecker, M. "Free Flight Testing of Novel Compliant Spines for Passive Wing Morphing", AIAA Paper 2013-1516